Biomed Microdevices (2010) 12:187–195
DOI 10.1007/s10544-009-9374-9

Inertial microfluidics for *sheath-less* high-throughput flow cytometry

Ali Asgar S. Bhagat · Sathyakumar S. Kuntaegowdanahalli · Necati Kaval · Carl J. Seliskar · Ian Papautsky

Published online: 28 November 2009

Abstract Flow cytometer is a powerful single cell analysis tool that allows multi-parametric study of suspended cells. Most commercial flow cytometers available today are bulky, expensive instruments requiring high maintenance costs and specially trained personnel for operation. Hence, there is a need to develop a low cost, portable alternative that will aid in making this powerful research tool more accessible. In this paper we describe a *sheath-less*, on-chip flow cytometry system based on the principle of Dean coupled inertial microfluidics. The design takes advantage of the Dean drag and inertial lift forces acting on particles flowing through a spiral microchannel to focus them in 3-D at a single position across the microchannel cross-section. Unlike the previously reported micro-flow cytometers, the developed system relies entirely on the microchannel geometry for particle focusing, eliminating the need for complex microchannel designs and additional microfluidic plumbing associated with sheath-based techniques. In this work, a 10-loop spiral microchannel 100 μm wide and 50 μm high was used to focus 6 μm particles in 3-D. The focused particle stream was detected with a laser induced fluorescence (LIF) setup. The microfluidic system was shown to have a high throughput of 2,100 particles/sec. Finally, the viability of the developed technique for cell counting was demonstrated using SH-SY5Y neuroblastoma cells. The passive focusing principle and the planar nature of the described design will permit easy integration with existing lab-on-a-chip (LOC) systems.

Keywords Microfluidics · Flow cytometry · Cell counting

A. A. S. Bhagat · S. S. Kuntaegowdanahalli · I. Papautsky (✉)
Department of Electrical and Computer Engineering,
University of Cincinnati,
814 Rhodes Hall, ML030,
Cincinnati, OH 45221, USA
e-mail: ian.papautsky@uc.edu

N. Kaval · C. J. Seliskar
Department of Chemistry, University of Cincinnati,
Cincinnati, OH 45221, USA

1 Introduction

Flow cytometry is a powerful cell analysis technique that permits multi-parametric study of suspended cells and provides a rapid and accurate tool for single cell analysis. In this technique a laser beam is focused on fluorescently labeled cells, passing sequentially through the interrogation region at a rate of thousands of cells per second. By capturing the scattered light and fluorescence emission, physical and chemical properties of the cells can be determined and cells can be sorted and counted. This high throughput technique is used in a variety of biomedical (Harding et al. 2000; Boeck 2001) and clinical diagnostic applications (Stein et al. 1992; Fenili and Pirovano 1998) including bacterial analysis (Gunasekera et al. 2000), analysis of cell cycle and apoptosis (Darzynkiewicz et al. 2001), detection of minimal residual disease (MRD) in leukemia cases (Deptala and Mayer 2001), and enumeration of CD4+ T-cells in HIV diagnosis (Cheng et al. 2007). Additionally, flow cytometers can be used purely in cell sorting applications (Melamed et al. 2000). Commercial flow cytometers, however, are bulky, expensive, and require specially trained maintenance personnel (Huh et al. 2005).

The high demand for low cost and portable cell analysis techniques for biomedical and clinical applications has led to the development of a number of miniaturized microfluidic flow cytometer systems. These systems offer a number of advantages, including smaller volumes, increased sensitivity, lower fabrication costs, portability, and

the possibility of integrating several functionalities on a single chip (Mao et al. 2009). Additionally, multiple flow cytometers can be fabricated in parallel on a single chip, thus facilitating very high throughput analysis.

A critical aspect of the flow cytometry technique is to ensure that cells traverse the interrogation region one at a time. Conventional flow cytometers achieve such 3-D focusing of the sample cell stream using complex fluidic systems with co-axial injection flow chambers and sheath fluids. Such fluidic systems, however, are complicated, bulky, and expensive to manufacture. On the microscale, the inherent laminar nature of microfluidic flows can be exploited to achieve 3-D focusing of cells in simple microchannel geometries that can be fabricated with standard soft lithography techniques. Some of the techniques employed to focus cells in microfluidic systems include the use of narrow constricted channels (Eyal and Quake 2002; Fu et al. 1999), focusing sheath flows (Lancaster et al. 2005; Sundararajan et al. 2004), and dielectrophoresis (Lin et al. 2004). For example, Fu et al. (1999) employed 3 μm wide channel to achieve fluorescence activated sorting of *E. coli* cells. Although, many other groups have successfully demonstrated focusing using similar techniques, the use of narrow channels suffers from critical drawbacks associated with channel clogging and significant pressure drops. Moreover, the use of constricted channels is not ideal for applications having a broad range of cell sizes.

The majority of microfluidic flow cytometers reported to date employ sheath flows to focus cells into a narrow stream. These devices can be broadly classified based on the dimensions used to generate the focusing, *i.e.* 2-D or 3-D. In 2-D focusing, the cell stream is focused at the center of the channel in the horizontal direction (parallel to the device plane) by the sheath fluids flowing on either side. The width of the cell stream is controlled by adjusting the flow rates of the sheath fluids. Since the cell stream is only focused along the horizontal plane, more than one cell can enter the interrogation region at any point of time, causing large measurement errors (Mao et al. 2009). Another problem associated with the 2-D focusing scheme is the variation in output signal intensities due to particles passing the interrogation region at different positions along channel height.

In 3-D focusing, the cell stream is focused both horizontally and vertically. Sundararajan et al. (2004) demonstrated a vertical chamber with six sheath inlets to focus the sample stream in the middle of the channel. However, this approach requires fabrication of multi-layer 3-D structures which are quite complex and difficult to manufacture in bulk. Thus, most of the microfluidic cytometer systems reported to date are sheath-based systems that require additional on-chip fluidic components such as reservoirs, micro-valves, and micro-pumps, which increase system complexity. Further, the high velocity sheath flows introduce additional stresses on cells flowing through the sample stream. Hence, clear advantages can be gained from microscale sheath-less 3-D focusing.

Recently, our group demonstrated a 3-D hydrodynamic focusing in spiral microchannels using the principle of Dean coupled inertial microfluidics (Bhagat et al. 2008a; Kuntaegowdanahalli et al. 2009). The developed design uses spirally-shaped microchannels for two-dimensional hydrodynamic focusing of particles. The technique relies entirely on the microchannel geometry for functionality, eliminating the need for complex channel geometries and other plumbing controls associated with sheath-based systems. Using such hydrodynamic focusing to define the 3-D sample stream in a flow cytometer can lead to a passive microfluidic system with simple microchannel geometry and easy (low-cost) device fabrication.

In this work, we describe a high-throughput *sheath-less* microscale flow cytometer using inertial microfluidics to focus particles into a single ordered stream. Figure 1 schematically illustrates the concept of the developed cytometer. The design consists of a spiral microchannel with a single inlet and outlet port. The randomly distributed particles at the inlet equilibrate into a focused stream at the channel outlet under the influence of inertial lift forces coupled with Dean drag. The design thus achieves *sheath-less* 3-D particle focusing eliminating the need for additional microfluidic plumbing. Absence of channel constrictions eliminates problems arising from channel clogging, enabling high-throughput. Based on the results presented in this work, we believe microscale flow cytometers can be designed for microscale particles (e.g., cells), and possibly nanoscale particles (e.g., bacteria, viruses), over a wide dynamic range.

2 Design principle

Neutrally buoyant particles (or cells) suspended in a fluid flowing through a microchannel experience a drag force due to the viscous nature of the carrier fluid which entrains particles *along* the flow streamlines. In addition to the drag force, neutrally buoyant particles (or cells) with sizes comparable to the microchannel dimensions experience significant inertial lift forces, leading to their migration *across* the flow streamlines and thus the microchannel cross-section. The parabolic nature of the laminar velocity profile in Poiseuille flow produces an inertial lift force induced by shear gradient that drives particles away from the microchannel center towards the microchannel walls (Bhagat et al. 2008a; Di Carlo et al. 2007). As particles migrate closer to the channel wall, an asymmetric rotational wake around particles is disturbed by the presence of

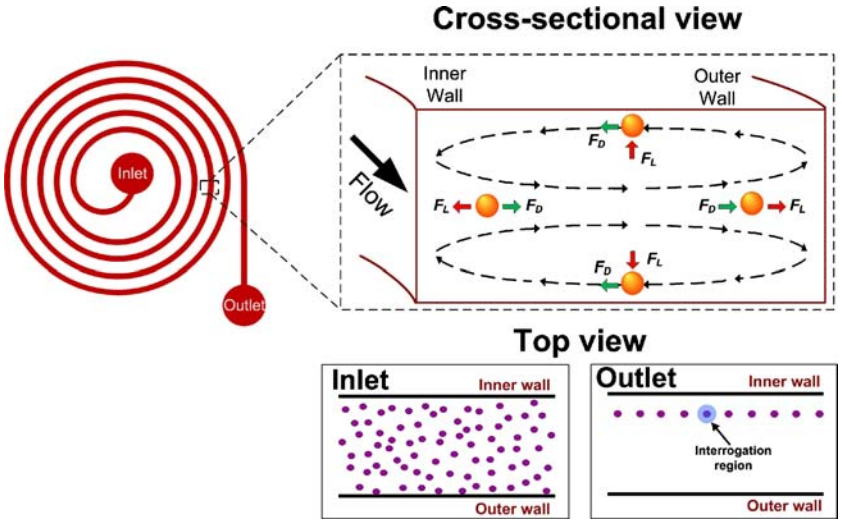

Fig. 1 Schematic of the spiral microfluidic design illustrating sheathless 3-D particle focusing for flow cytometry applications. Neutrally buoyant particles flowing in curvilinear channels experience a combination of inertial lift (F_L) and Dean drag (F_D) forces. The microchannel cross-sectional view illustrates direction of these forces acting on particles at various positions across the microchannel cross-section. As a result, the randomly dispersed particles at the channel inlet focus into a single ordered stream at the channel outlet facilitating counting (*top view*)

channel walls, generating a wall-induced lift force that drives particles away from the wall (Bhagat et al. 2008a; Di Carlo et al. 2007). These oppositely directed forces exert a net lift force (F_L) on the particles equilibrating them into focused streams around the microchannel perimeter (Asmolov 1999; Di Carlo et al. 2007).

Segre and Silberberg (1961, 1962) were the first to report this effect demonstrating that a uniformly distributed suspension of neutrally buoyant particles form a narrow band at ~0.2D from the channel walls in a circular channel of diameter D. In our recent work, we demonstrated this effect in square and rectangular microchannels for Re<50 flows (Bhagat et al. 2008b, 2009).

The preferential focusing of particles occurs when a_p/L_C> 0.07 (where a_p is particle diameter and L_C is the characteristic length) (Bhagat et al. 2008b, 2009). Typically, hydraulic diameter (D_h=4A/P for a microchannel with cross-sectional area A and perimeter P) is used as the characteristic length scale of a microchannel with non-circular cross-section. For high aspect ratio microchannels ($AR = h/w$ >1), however, the characteristic length (L_C) is the narrowest channel dimension (Bhagat et al. 2008b, 2009).

The net lift force acting on a particle can be calculated as a function of particle position as

$$F_L = \frac{2\rho U_f^2 a_p^4}{L_C^2} \tag{1}$$

where ρ is the fluid density, U_f is the average flow velocity, and a_p is the particle (cell) diameter. Thus, the lift force is a function of microchannel cross-section, flow velocity, and particle (cell) size.

Using Stoke's Law, microchannel length required for particle equilibration (L_I) can be now calculated as

$$L_I = \frac{3\pi\mu}{2\rho U_f}\left(\frac{L_C}{a_p}\right)^3 \tag{2}$$

Thus, the microchannel length required for particles to migrate to the equilibrium positions varies as $1/(a_p/L_C)^3$, which indicates that a small change in the particle size or the channel characteristic dimension can significantly impact the channel length required for migration. Increasing the a_p/L_C ratio accelerates particle migration leading to particle focusing within significantly shorter channel lengths.

In spiral microchannels, in addition to lift forces particles (cells) experience a drag force due to the transverse Dean flows. Due to the curvilinear channel geometry, the centrifugal acceleration directed radially outward leads to the formation of two counter-rotating vortices known as Dean vortices in the top and bottom halves of the channel (Dean 1928; Ookawara et al. 2004). The magnitude of these secondary flows is quantified by a dimensionless Dean number (De) given by:

$$De = \mathrm{Re}\sqrt{\frac{D_h}{2R}} \tag{3}$$

where Re is the flow Reynolds number and R is the radius of curvature of the channel. The average Dean velocity for a given De is given by

$$\overline{U}_{Dean} = 1.8 \times 10^{-4} De^{1.63} \tag{4}$$

and the Dean drag force (F_D) exerted on particles can then be obtained using Stokes' Law

$$F_D = 3\pi\mu\overline{U}_{Dean}a_p = 5.4 \times 10^{-4}\pi\mu De^{1.63}a_p \quad (5)$$

Particles dispersed in a spiral microchannel get entrained in one of the two Dean vortices are forced to follow fluid movement, as shown in Fig. 1. The Dean drag force and the inertial lift forces tend to dominate the migration of neutrally buoyant particles with $a_p/L_C > 0.07$. As mentioned previously, the inertial net lift force F_L acts to equilibrate particles along the microchannel perimeter in eight stable equilibrium positions (Bhagat et al. 2008b, 2009; Di Carlo et al. 2007). Particles flowing near the top and bottom microchannel walls experience strong lateral flows due to Dean drag F_D and migrate towards the inner microchannel wall (Fig. 1). Near the outer microchannel wall, the net lift force acts along the direction of F_D and the particles continue to follow the Dean vortices independent of their size. However, near the inner microchannel wall, F_L and F_D act in opposite directions leading to particle equilibration and formation of a focused stream (Bhagat et al. 2008a). Thus, adding a component of Dean drag reduces the number of equilibrium positions to just one, near the inner microchannel wall. In this work, this 3-D hydrodynamic focusing is exploited for *sheath-less* high-throughput flow cytometry application.

3 Methods

3.1 Microchannel design and fabrication

The spiral microchannels were fabricated in polydimethylsiloxane (PDMS, Sylgard 184, Dow Corning, Midland, MI, USA). The design consisted of spiral microchannel with an inlet and outlet. The width and height of the microchannel were varied depending on the particle size to satisfy the $a_p/L_C > 0.07$ criterion. For the 6 μm diameter particle tested in this work, a 10-loop 100 μm×50 μm (W×H) spiral geometry was fabricated. The SH-S5Y5 neuroblastoma cells with a mean diameter of 15 μm were tested in a 5-loop 500 μm×120 μm (W×H) microchannel. The total lengths of the microchannels were ~25 cm and 40 cm respectively.

The spiral microchannels were fabricated using standard soft lithography methods (Bhagat et al. 2007). Briefly, a thick layer of SU-8 photoresist (2075, Microchem Corp., Newton, MA, USA) was patterned on a single-side polished 3″ silicon wafer using conventional photolithography techniques. PDMS prepolymer mixed in a 10:1 ratio with the curing agent was then cast on the SU-8 master to replicate microchannel features. After curing, the PDMS mold was peeled from the SU-8 master and O_2 plasma bonded to a 1 mm thick glass slide to complete the microchannel. Input and output ports were cored using a 14 gauge syringe needle prior to bonding.

3.2 Characterization

To experimentally evaluate particle focusing, a 5 cc syringe driven using syringe pumps (NE-1000X, New Era Pump Systems, Wantagh, NY, USA) was used to pump the sample through the microchannel. The syringe was filled with commercially available 6 μm (σ=0.6 μm) diameter fluorescently labeled polystyrene particles (Bangs Laboratories, Fishers, IN, USA) dispersed in DI water (0.05% volume fraction). Varying concentrations of the same solution was also used to demonstrate particle counting. To confirm particle focusing, high speed images of the channel were captured at various locations downstream during testing using an inverted epi-fluorescence microscope (Olympus IX71, Olympus Inc., Center Valley, PA, USA) equipped with a 12-bit CCD camera (Retiga EXi, QImaging, Surrey, BC, CA). A stack of 300 images (Z-stacked) from each location was then overlaid to create composite images confirming particle focusing.

Figure 2 shows a schematic illustration of the laser-induced fluorescence (LIF) setup used to detect and count particles. The spiral microfluidic devices were mounted on an inverted microscope (TE2000U, Nikon Inc., Melville, NY, USA) equipped with a 20× objective (Plan Fluor ELWD 20× C, 0.45 NA, Nikon Inc., Melville, NY, USA). Both particles and cells were excited using epifluorescent excitation provided by a 488 nm argon laser (50 mW, CVI Melles Griot, Albuquerque, NM, USA). The laser output power was adjusted using a variable neutral density filter (Thorlabs, Newton, NJ, USA). The emitted light was gathered by the same objective and projected onto the cathode of a PMT (H6780-20, Hamamatsu, Bridgewater, NJ, USA). The output of the PMT was sent to a current-to-voltage preamplifier (SR570, Stanford Research Systems, Sunnyvale, CA, USA), before being recorded by a custom LabVIEW data acquisition system (NI PCI 6036E National Instruments, Austin, TX, USA). The acquired signal was then analyzed for particle count and amplitude variation using a custom Perl code.

To demonstrate cell counting, SH-SY5Y neuroblastoma cells ~15 μm (σ=5 μm) in diameter were cultured in Opti-MEM medium (Invitrogen Corp., Carlsbad, CA, USA) containing 10% fetal bovine serum supplemented with L-glutamine. The culture was maintained at 37°C in a humidified atmosphere containing 5% (*v*/*v*) CO_2. Cells were cultured in sterile 25 cm^2 flasks (Corning, Lowell, MA, USA). Cells were sub-cultivated (1:4) three times a week and media was replaced every 48 h. Sub-confluent

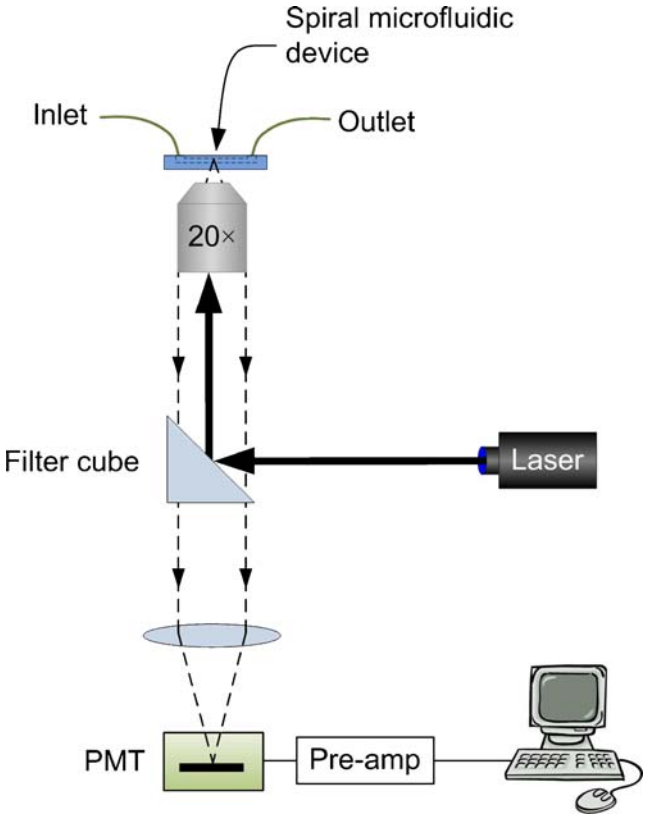

Fig. 2 Schematic diagram illustrating the LIF set-up for particle detection and counting. The particles are excited using a 488 nm argon laser beam focused using a 20× objective. The emitted light is projected onto the cathode of a PMT and recorded using a custom LabVIEW data acquisition system

monolayers were dissociated with 0.01% trypsin and 5.3 mM EDTA solution, re-suspended in fresh basal media with 5% serum for further subculture. Cells were never allowed to reach 100% confluency. Prior to testing, the cells were mixed together and diluted in 1× phosphate buffered saline (PBS) solution (0.05% volume fraction). The cells were labeled with CellTracker™ Green (Invitrogen Corp., Carlsbad, CA, USA) for detection. The PDMS based devices were thoroughly flushed with PBS and antibiotics (1× PSN) before running the cell mixture and all experiments were conducted in a sterile environment.

4 Results and discussion

Figure 3(a) illustrates the fabricated 10-loop 100 μm×50 μm (W×H) spiral microchannel in PDMS. To confirm 3-D particle focusing, the fabricated devices were tested for a wide range of flow rates, $0.05 \leq De \leq 2.3$. The flow was limited to $De \leq 2.3$, which corresponds to the maximum input flow of 100 μL/min or $Re \sim 20$. For the given microchannel dimensions, the 6 μm diameter particles yield $a_P/L_C = 0.12$ (>0.1), which satisfies the condition for particle equilibration. Thus, the lift forces align these particles in the eight equilibrium positions around the channel periphery, with the strong lateral Dean flows at the top and bottom of the microchannel reducing the equilibrium positions further to just one near the inner wall as described in the design principle section.

The composite fluorescent images illustrating particle distribution across the microchannel inlet and outlet sections of the 10-loop microchannel at $De = 2.3$ are presented in Fig. 3(b–c). The uniformly dispersed 6 μm diameter particles at the inlet (Fig. 3(b)) focus into a single stream near the inner microchannel wall at the outlet (Fig. 3(c)) under the influence of Dean-coupled inertial migration. The high-speed image (25 μs exposure, Fastec TroubleShooter camera, Fastec Imaging Inc., SD, USA) in Fig. 3(d) clearly

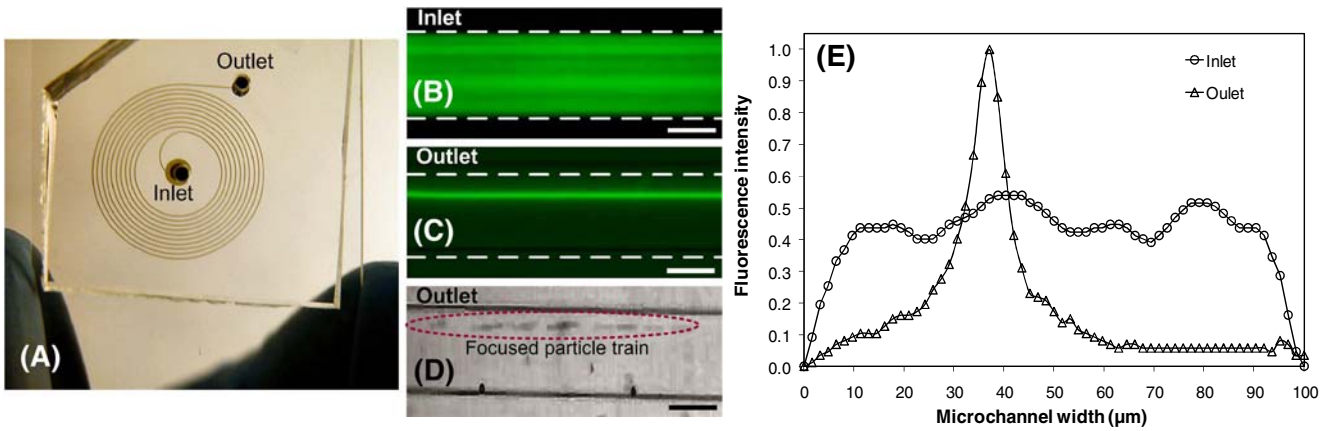

Fig. 3 (**a**) Photograph of the 10-loop spiral microchannel fabricated in PDMS. (**b**–**c**) Fluorescent images illustrating distribution of 6 μm particles across the microchannel inlet and outlet for $De = 2.3$. The result confirms 3-D particle focusing at the outlet of the spiral microchannels using inertial forces. (**d**) High speed (25 μs exposure) bright field image showing a train of focused particles near the inner microchannel wall. (*Scale bar*, 50 μm) (**e**) Corresponding fluorescence line-scans indicating the normalized distribution of 6 μm particles across the channel inlet and outlet

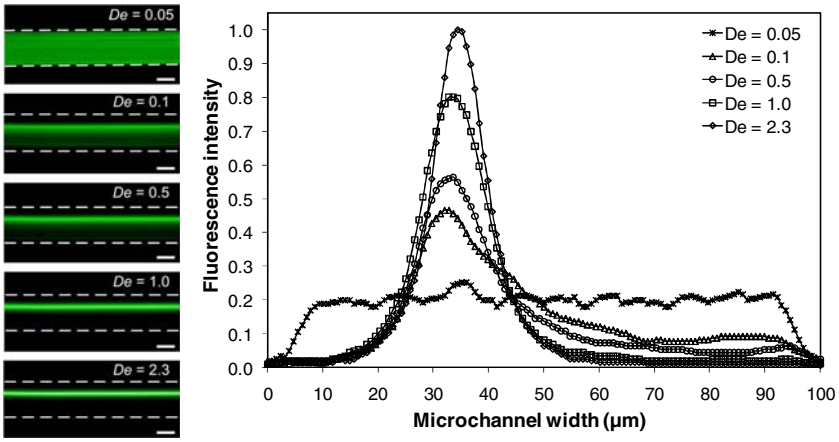

Fig. 4 Effect of *De* on sheathless 3-D particle focusing of 6 μm diameter particles across the 100×50 μm^2 microchannel outlet. Line-scans across microchannel outlet show the normalized particle distribution for increasing *De*. In all fluorescent image panels bright white lines indicate approximate position of microchannel walls. (*Scale bar*, 50 μm)

reveals a focused train of particles near the inner wall at the microchannel outlet. The normalized distribution of the particles at the microchannel inlet and outlet is shown in Fig. 3(e).

Inertial focusing of particles in a single stream in spiral microchannels of finite length is highly dependent on the fluid flow rate (U_f). Figure 4 illustrates the effect of increasing *De* on particle focusing. At lower Dean number (De=0.05), due to significantly weak inertial forces and Dean forces, the 6 μm diameter particles remain evenly distributed across the microchannel cross-section indicating little migration. Increasing the flow rate to $0.1 \leq De \leq 0.5$ increases the lift force which permits particles to overcome the viscous drag. The particles begin migrating across the microchannel cross-section towards the equilibrium positions and form focused streams. The Dean forces further reduce the equilibrium positions to just one near the inner microchannel wall. However, as the Dean forces are not very high, not all particles are tightly focused into a single stream by the time the flow reaches the outlet, as confirmed by the corresponding fluorescent images and line-scans. This weak particle focusing (FWHM~20 μm) within the microchannel will lead to large variations in the CCD output, yielding a large coefficient of variation due to the poor recorded signal. Coefficient of variation is a normalized measure of dispersion of signal and is defined as the ratio of the standard deviation σ_s to the mean μ_s ($\mathrm{CV} = \sigma_s/\mu_s \times 100\%$).

It is critical to ensure that all particles experience strong focusing in 3-D. This can be achieved by either increasing the microchannel length to allow all particles to focus or by further increasing the flow rate and speeding the particle focusing in shorter distances. The magnitude of these Dean vortices increases with increasing fluid velocity due to the higher centrifugal force acting on the fluid. Increasing the flow rate to De>1.0 results in tighter particle focusing near the inner microchannel walls (FWHM~10 μm) as confirmed by the fluorescent image and line-scan. Increasing the flow rate further to De>1.0 causes the focused particle stream to move away from the channel wall at increasing *De*, indicating the dominance of the Dean force (Kuntaegowdanahalli et al. 2009). However, the particle stream still remains tightly focused with a shift in the interrogation region position.

To demonstrate the application of the developed technique to *sheath-free* flow cytometry, the microfluidic device was tested using the LIF setup. The particles were tested at De=2.3, and the focused particle stream was aligned with the 488 nm laser beam. The 3-D focused particle stream was imaged using a 20× objective, yielding an interrogation region of ~10 μm in diameter, thus exciting all the 6 μm diameter fluorescent particles. The size of the interrogation region can be increased or decreased by using appropriate objectives, with the suggested interrogation region diameter ~2× the particle diameter to warrant the detection of all particles. Figure 5(a) shows a typical 100 ms fluorescent peak scan recorded using the LIF setup. Each peak represents a single 6 μm fluorescent bead passing through the interrogation region. Figure 5(b) shows an amplified 10 ms interval of the fluorescent signal scan indicating little variation, thus confirming excellent 3-D particle focusing. Particle count was recorded for 3 s at a sampling rate of 300 kHz using a LabVIEW data acquisition system. The recorded signal was then analyzed for particle count using a custom Perl program. For the signal presented in the figure, we detected 6,288 particles in 3 s, yielding a significantly high throughput of ~2,100 s^{-1}. The throughput of the system can be further increased by using more concentrated inlet solutions (>0.1% volume fraction).

To test the accuracy of the cytometer, the system was tested with different inlet particle concentrations. The inlet particle count was confirmed using a hemocytometer and matched the recorded count within 3% (data presented in Table 1). The recorded signals also displayed good uniformity, with low variability (CV<20%) and very high throughput. These results are a significant improvement

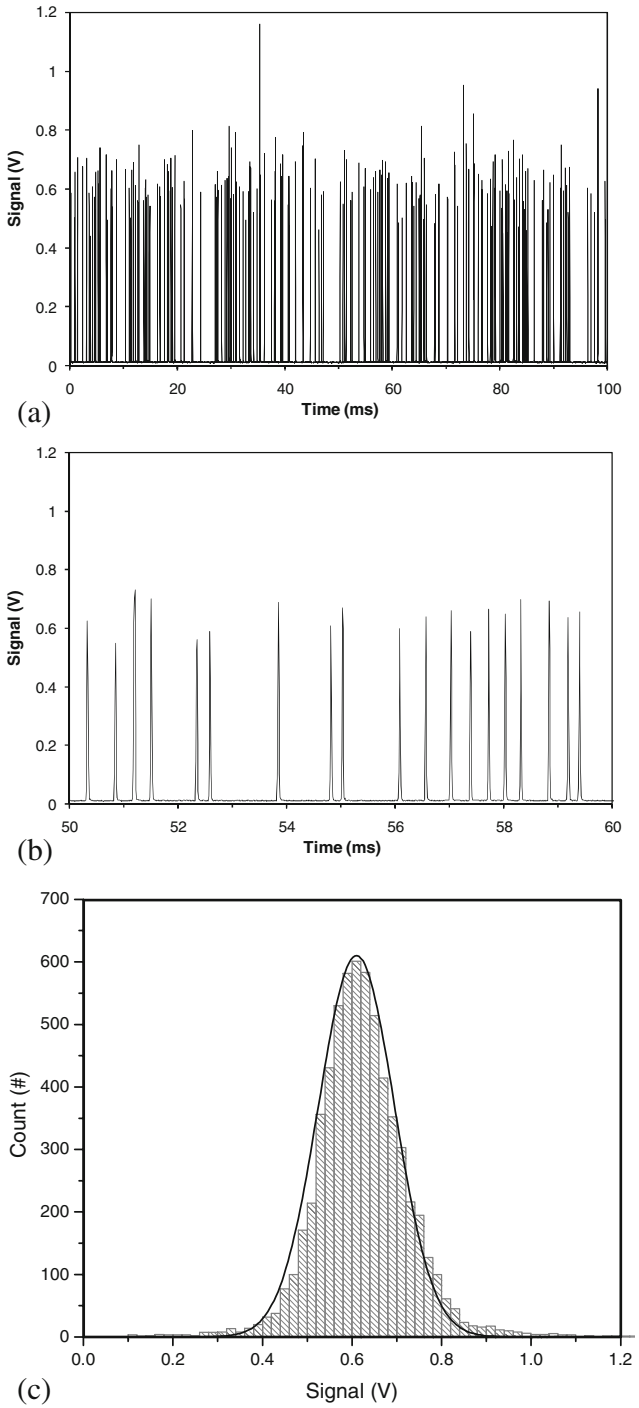

Fig. 5 (**a**) A 100 ms region of the fluorescent signal scan recorded using the LIF system. Each peak represents a single 6 μm fluorescent bead passing through the detection region. The throughput of the system was ~2,100 particles/s. (**b**) Amplified 10 ms interval of the fluorescent signal scan indicating little variation and confirming tight 3-D particle focusing. (**c**) Histogram of the fluorescent peak amplitude indicating a Gaussian-like distribution. The signal exhibits an 18% coefficient of variation (CV) indicating a tightly focused particle stream

Table 1 Summary of experimental results indicating the inlet and measured particle count for varying concentrations

S. No	Concentration ($\times 10^5$/mL)		Particle flux (s^{-1})	% Error	Coefficient of variance (%)
	Inlet	Measured			
1	0.8	0.784	130	3.0	20
2	12.2	12.5	2,096	3.0	18
3[a]	0.3	0.298	498	0.4	58

[a] SH-SY5Y neuroblastoma cells test

over the previous reports for sheath-based microscale flow cytometers (Mao et al. 2009), confirming superior particle focusing capability with reduced system complexity. Figure 5(c) presents a histogram of the fluorescent peak amplitude for the signal presented in Fig. 5(a) indicating a Gaussian-like distribution. The signal exhibits a CV=18% indicating a tightly 3-D focused particle stream. The CV is lower compared to other reported microscale flow cytometers which usually focus the samples into thin sheets (2-D) (Mao et al. 2009; Wang et al. 2004).

Finally, application of the developed technique to cell counting was demonstrated using SH-SY5Y neuroblastoma cells. Based on the size of these cells (a_p=15 μm), the SH-S5Y5 cell samples were tested in a 5-loop 500 μm×120 μm (W×H) microchannel at *De*=12.2. Figure 6 presents typical a 10 ms interval of the fluorescent signal scan recorded using the LIF setup. Each peak represents a single cell passing through the interrogation region. The focused cell stream was imaged using a 10× objective, yielding an interrogation region of ~20 μm in diameter. The large variations in the signal amplitude (CV~58%) is attributed to the large variation in the cell sizes (σ=5 μm) which results in focusing the cells in a band (indicated in the inset

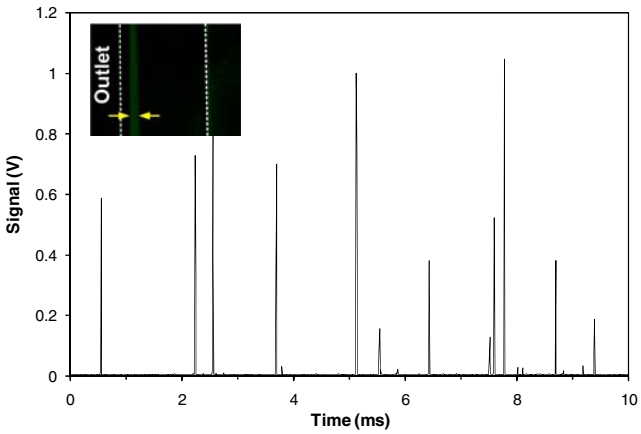

Fig. 6 A 10 ms region of the fluorescent signal scan recorded using the LIF system. Each peak represents a single SH-S5Y5 cell passing through the detection region. The large variation in the peak signal is attributed to the significant variation in the cell sizes

fluorescent image) rather than a single stream. Even with such large CV, the inlet cell count matched the recorded count within 1% (data presented in Table 1), indicating high device accuracy which is a critical requirement of all flow cytometers.

The developed flow cytometer offers the key advantage of considerably high throughput over other reported microscale flow cytometers. The ~2,100 s^{-1} particle throughput of this work can be increased even further by using a more concentrated particle suspension at the inlet. Since only a 0.05% volume fraction was used in this work, the particle count may be increased even further, nearly an order of magnitude, by simply increasing the volume fraction and fluid flow rates (volume fractions of 0.1–0.3% have been reported by others (Di Carlo et al. 2008)). Typical microscale flow cytometers report a throughput of ~100 s^{-1}. Gawad et al. (2001) reported a cytometer based on principle of micro Coulter particle counting (μCPC) with screening rates of ~100 samples s^{-1}. Tung et al. (2004) reported sheath-based flow cytometer with integrated PIN photodiodes with throughputs as high as 500 s^{-1}. Recently, Simonnet and Groisman (2006) reported a high-throughput high-resolution flow cytometer using sheath-based 3-D particle focusing. The 17,000 particles s^{-1}throughput of their system is the highest reported for any microscale flow cytometer to date. However, the volume throughput of their system is very low and is calculated to be ~1 mL/hr. The cytometer developed in this work offers the advantage of higher volume throughput, critical for large sample analysis. For the experiments with cells, the volume throughput of our systems is ~2 mL/min, thus significantly reducing the analysis time. The technique is able to focus the sample stream in channels with width and heights at least 10 times the particle/cell diameter. The passive sheath-less principle and the planar nature of the design will permit easy integration with existing lab-on-a-chip components, envisaging numerous applications in high-throughput cell counting.

5 Conclusions

In this work, design of a *sheath-less* microfluidic cytometer based on the principle of Dean coupled inertial microfluidics for particle/cell counting was reported. The developed device is planar and thus simple to fabricate and integrate with other components of a LOC. A 10-loop spiral microchannel was employed to achieve 3-D focusing of fluorescently labeled 6 μm particles without any additional sheath fluids. The single ordered stream of 6 μm particles were then detected and counted using a LIF system. The recorded signal intensities displayed good uniformity (CV< 20%), confirming excellent 3-D particle focusing. The throughput of the device was shown to be ~2,100 particles/sec and this can be further increased by using concentrated solutions. Since the particle focusing in this technique is dependent on the ratio of Dean drag and inertial lift forces, a wide range of particle sizes can be analyzed in single microchannel design. The viability of the developed technique to cell counting applications was demonstrated by using a suitably designed spiral channel to count SH-SY5Y neuroblastoma cells. Finally, the technique is passive relying entirely on the microchannel geometry for functionality, eliminating the need for complex channel geometries or additional plumbing controls associated with sheath-based systems.

Acknowledgements This work was supported by the University of Cincinnati Institute for Nanoscale Science and Technology and the National Institute of Occupational Safety and Health (NIOSH) Health Pilot Research Project Training Program of the University of Cincinnati Education and Research Center (T42/OH008432-04). The authors are also grateful to Dr. Girish Kumar for providing cells for the experiments.

References

E.S. Asmolov, J. Fluid Mech. **381**, 63 (1999)
A.A.S. Bhagat, S.S. Kuntaegowdanahalli, I. Papautsky, Lab Chip **8**, 1906 (2008a)
A.A.S. Bhagat, S.S. Kuntaegowdanahalli, I. Papautsky, Phys. Fluids **20**, 101702 (2008b)
A.A.S. Bhagat, S.S. Kuntaegowdanahalli, I. Papautsky, Microfluid. Nanofluid. **7**, 217 (2009)
A.A.S. Bhagat, E.T.K. Peterson, I. Papautsky, J. Micromech. Microeng. **17**, 1017 (2007)
G. Boeck, Int. Rev. Cytol. **204**, 239 (2001)
X. Cheng, D. Irimia, M. Dixon, K. Sekine, U. Demirci, L. Zamir, R.G. Tompkins, W. Rodriguez, M. Toner, Lab Chip **7**, 170 (2007)
Z. Darzynkiewicz, E. Bedner, P. Smolewski, Semin. Hematol. **38**, 179 (2001)
W.R. Dean, Phil. Mag. Ser. **5**, 673 (1928)
A. Deptala, S.P. Mayer, Methods Cell Biol. **64**, 385 (2001)
D. Di Carlo, D. Irimia, R.G. Tompkins, M. Toner, Proc. Natl. Acad. Sci. USA **104**, 18892 (2007)
D. Di Carlo, J.F. Edd, D. Irimia, R.G. Tompkins, M. Toner, Anal. Chem. **80**, 2204 (2008)
S. Eyal, S.R. Quake, Electrophoresis **23**, 2653 (2002)
D. Fenili, B. Pirovano, Clin. Chem. Lab. Med. **36**, 909 (1998)
A.Y. Fu, C. Spence, A. Scherer, F.H. Arnold, S.R. Quake, Nature Biotech. **17**, 1109 (1999)
S. Gawad, L. Schild, P. Renaud, Lab Chip **1**, 76 (2001)
T.S. Gunasekera, P.V. Attfield, D.A. Veal, Appl. Environ. Microbiol. **66**, 1228 (2000)
C.L. Harding, D.R. Lloyd, C.M. McFarlane, M. Al-Rubeai, Biotechnol. Prog. **16**, 800 (2000)
D. Huh, W. Gu, Y. Kamotani, J.B. Grotberg, S. Takayama, Physiol. Meas. **26**, 73 (2005)
S.S. Kuntaegowdanahalli, A.A.S. Bhagat, G. Kumar, I. Papautsky, Lab Chip **9**, 2973 (2009)
C. Lancaster, A. Kokoris, M. Nabavi, J. Clemmens, P. Maloney, J. Capadanno, J. Gerdes, C.F. Battrell, Methods **37**, 120 (2005)

C.H. Lin, G.B. Lee, L.M. Fu, B.H. Hwey, J. Microelectromech. Syst. **13**, 923 (2004)
X. Mao, S.C.S. Lin, C. Dong, T.J. Huang, Lab Chip **9**, 1583 (2009)
M.R. Melamed, T. Lindmo, M.L. Mendelsohn, *Flow cytometry and sorting* (Wiley-Liss, New York, 2000)
S. Ookawara, R. Higashi, D. Street, K. Ogawa, Chem. Eng. J. **101**, 171 (2004)
G. Segre, A. Silberberg, Nature **189**, 209 (1961)
G. Segre, A. Silberberg, J. Fluid. Mech. **14**, 136 (1962)
C. Simonnet, A. Groisman, Anal. Chem. **78**, 5653 (2006)
D.S. Stein, J.A. Korvick, S.H. Vermund, J. Infect. Dis. **165**, 352 (1992)
N. Sundararajan, M.S. Pio, L.P. Lee, A.A. Berlin, J. Microelectromech. Syst. **13**, 559 (2004)
Y.C. Tung, M. Zhang, C.T. Lin, K. Kurabayashi, S.J. Skerlos, Sens. Actuators B **98**, 356 (2004)
Z. Wang, J. El-Ali, M. Engelund, T. Gotsaed, I.R. Perch-Nielsen, K.B. Mogensen, D. Snakenborg, J.P. Kutter, A. Wolff, Lab Chip **4**, 372 (2004)